Articles

Electronic Localization Due to Fluorine in $YBa_2Cu_3O_xF_y$ Superconducting Materials

Keu Hong Kim*, Don Kim†, Seung Koo Cho, Yong Wook Choi, Jong Sik Park, and Jae Shi Choi

Department of Chemistry, Yonsei University, Seoul 120-749. *Received September 11, 1989*

High-T_c superconducting materials, $YBa_2Cu_3O_xF_y$ with $x \leq 6.89$ and $0.25 \leq y \leq 0.35$, were prepared and studied by X-ray diffraction, magnetic susceptibility and resistivity measurement. Under given conditions, reproducible resistivities were obtained, which increased with increase in the amount of fluorine. The introduced fluorine atoms were found to be localized in pyramidal Cu-O units rather than in Cu-O chains. It is suggested that the localized fluorine atom increases the electronic localization of the superconducting electrons.

Introduction

It is helpful to know whether the fluorine atoms introduced into superconducting $YBa_2Cu_3O_x$ are substituted for oxygen atoms in the pyramidal Cu-O or the chain Cu-O. The Cu-O vibrations in the superconducting Y-Ba-Cu-O system have been reported to be consisted of Cu-O bending, pyramidal Cu-O stretching and chain Cu-O stretching vibrations based on Raman spectroscopy studies.[1-6] For example, Macfarlane *et al.*[1] observed ten Raman active phonon modes with frequencies from 153 to 640 cm^{-1} in sintered polycrystalline $YBa_2Cu_3O_7$. The Raman lines at 335, 500 and 601 cm^{-1} have been assigned to Cu-O bending, pyramidal Cu-O stretching and chain Cu-O stretching vibrations, respectively. The symmetric pyramidal Cu-O stretching and asymmetric pyramidal Cu-O stretching vibrational modes have also been observed at 502 and 589 cm^{-1} respectively in $YBa_2Cu_3O_x$ superconductors.[2,3] A mode at 337 cm^{-1} was also observed in fluorinated $YBa_2Cu_3O_x$ (x = 6.57-6.47) and it was assigned to Cu-O bending vibration.[4]

Cho *et al.*[4] prepared normal and fluorinated Y123 samples and compared their Raman spectra. They found that all of the Raman band frequencies of the samples are same (mainly 337, 501 and 600 cm^{-1}), irrespective of the fluorine doping level, but a new Raman line at 298 cm^{-1} appears in the fluorinated Y123. This line is not observed in normal superconducting $YBa_2Cu_3O_{6.67}$. The intensity of this peak increases as the fluorine fraction increases. From the increasing and decreasing intensities of the 298 cm^{-1} and other lines with the fluorine content, it is clear that the fluorine atom is in the pyramidal Cu-O unit rather than in the Cu-O chain, since Cu-O chains vibrate at frequencies higher than 298 cm^{-1}.

Tyagi *et al.*[7] have reported that fluorinated Y123 cannot be synthesized by sintering the mixture of normal Y123 and NH_4HF_2, because thermally stable BaF_2 phase was formed. But, Ovshinsky *et al.*[8] and Bhargava *et al.*[9] reported that flourinated Y123 can be synthesized by sintering the mixture of Y_2O_3, BaF_2 and CuO, and by that of Y_2O_3, $BaCO_3$, CuO and BaF_2, respectively.

In this paper, it is suggested from electron microprobe analysis, X-ray diffraction, magnetic susceptibility and resistivity measurement, and previous Raman spectroscopy data that the fluorine atom which is substituted for the oxygen atom in the pyramidal Cu-O unit localizes the superconducting electron.

Experimental

Sample Preparation and Analysis. $YBa_2Cu_3O_{6.89}$ was prepared from the following mixture: 0.5000 Y_2O_3, 2.000 $BaCO_3$ and 3.000 CuO. $YBa_2Cu_3O_{6.64}F_{0.25}$, $YBa_2Cu_3O_{6.59}F_{0.30}$ and $YBa_2Cu_3O_{6.54}F_{0.35}$ phases were also prepared in the same way starting from the following sets of mixture: 0.5000 Y_2O_3, 2.000 $BaCO_3$, 2.875 CuO and 0.1250 CuF_2; 0.5000 Y_2O_3, 2.000 $BaCO_3$, 2.850 CuO and 0.1500 CuF_2; 0.5000 Y_2O_3, 2.000 $BaCO_3$, 2.825 CuO and 0.1750 CuF_2. Each mixture was ball-mill-mixed, finely ground, calcined at 830 °C for 6 h in air, sintered at 900 °C for 5 h in air, annealed at 730 °C for 15 h in air, and then cooled to room temperature in air at a cooling rate of 30 °C/hr. The well mixed powder was pressed into a pellet under 49 MPa and the pellet was sintered at 900 °C for 10 h in air and then annealed at 500 °C for 6 h. After annealing, each sample was furnace-cooled to room temperature at a cooling rate of 30 °C/hr.

X-ray diffraction powder analyses were performed on a diffractometer (Philips, PW 1710, CuK_α) equipped with a curved graphite monochromator in the selected beam path. Rosen *et al.*[5] have published Raman spectra of high-T_c superconducting $YBa_2Cu_3O_x$ and the other possible impurity phase, $BaCuO_2$. They observed Raman spectra lines in the 630 to 640 cm^{-1} range due to this $BaCuO_2$ phase as well as for the superconducting $YBa_2Cu_3O_x$. Based on their findings, the $BaCuO_2$ phase can be identified more easily by Raman spectroscopy than by X-ray diffraction analysis. Since Raman lines at frequencies of 630-640 cm^{-1} were found for the present normal and fluorinated Y123 superconductors as well as for the $BaCuO_2$ phase, electron microprobe analyses (EPMA, JEOL JCX 333) were performed to see if microcrystals of the $BaCuO_2$ impurity phase were embedded in the larger normal and fluorinated Y123 polycrystals.

†Present address: General Education Department, Pusan National Institute of Technology, Yongdang-dong 100, Nam-gu, Pusan 608-080.

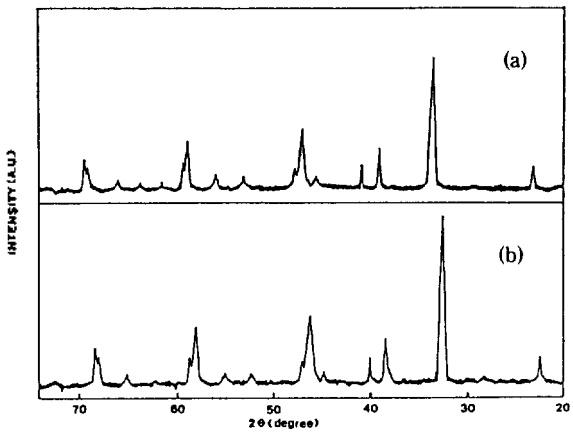

Figure 1. X-ray diffraction patterns of the $YBa_2Cu_3O_{6.89}$(a) and $YBa_2Cu_3O_{6.59}F_{0.30}$(b) superconductors.

Table 1. Cell Parameters for Various Samples

Sample	a(Å)	b(Å)	c(Å)
$YBa_2Cu_3O_{6.89}$	3.86 (±0.001)	3.90(±0.001)	11.78(±0.001)
$YBa_2Cu_3O_{6.64}F_{0.25}$	3.80(±0.001)	3.84(±0.001)	11.63(±0.001)
$YBa_2Cu_3O_{6.59}F_{0.30}$	3.79(±0.001)	3.83(±0.001)	11.60(±0.001)
$YBa_2Cu_3O_{6.54}F_{0.35}$	3.78(±0.001)	3.82(±0.001)	11.57(±0.001)

Magnetization Measurement. A polycrystalline sample was used for magnetization measurement. Magnetizations were measured by using a vibrating sample magnetometer (EG & G, Princeton Applied Research Co., Model 135) in a field of up to 5 KG at 80 K.

Resistivity Measurement. A sample of about 1.3 mm × 4.0 mm × 9.0 mm in size was cut from the pellet for resistance measurements by a standard four-probe ac technique. Copper wires were used as electrical leads and attached to the sample with indium. The current used to measure the electrical resistance was 5–30 mA, and the resolution of the voltage measurement was 10 μV. The resistance and transition temperature were not affected by the current in this range. The potential difference was measured with a lock-in amplifier (EG & G Co., PARC 5210) up to 10 μV on an IBM-PC/AT. The frequency was 110 Hz. The measured resistance was converted to resistivity using cell parameters. The temperature was measured with a copper-constantan thermocouple. A multiplexer board (PCLD 789 MUX; Advantech Co., Ltd.) and a 14-bit A/D converter (PCL 714; Advantech Co., Ltd.) were used to convert voltage into temperature, and the error range of temperature was ±0.01 °C.

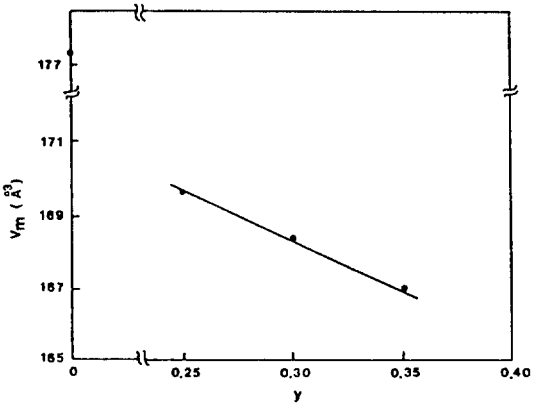

Figure 2. The unit cell volume(V_m) *vs.* fluorine atom contents for the fluorinated and normal superconducting $YBa_2Cu_3O_xF_y$.

Results and Discussion

Figure 1 shows typical powder X-ray diffraction patterns of the normal and fluorinated Y123 samples. Based on the diffraction patterns only, the fluorinated and normal Y123 samples are identified as essentially single phases with the layered perovskite structure. The X-ray powder diffraction data of the samples were successfully indexed on an orthorhombic cell and the phase of the present samples has been found to be an orthorhombic and oxygen-deficient perovskite with a chemical composition of $x = 6.89$ determined from redox titration.[10]. This long unit cell is responsible for the orthorhombic structure with an ordered array of Ba and Y. The substitution of fluorine atoms for oxygen atoms induces the unit cell parameter slightly shorter as shown in Table 1 as expected from the difference between the ionic radii of oxygen (124 pm) and fluorine (117 pm). Figure 2 shows the decrease in unit cell volume depending upon the substitution rate of fluorine in the fluorinated superconducting $YBa_2Cu_3O_xF_y$.

Figures 3 and 4 show homogeneous backscattered electron intensities which show no compositional zoning, a yttrium X-ray image indicating homogeneous Y-distribution and a part of yttrium X-ray profile showing no significant variation of yttrium content for the normal and fluorinated

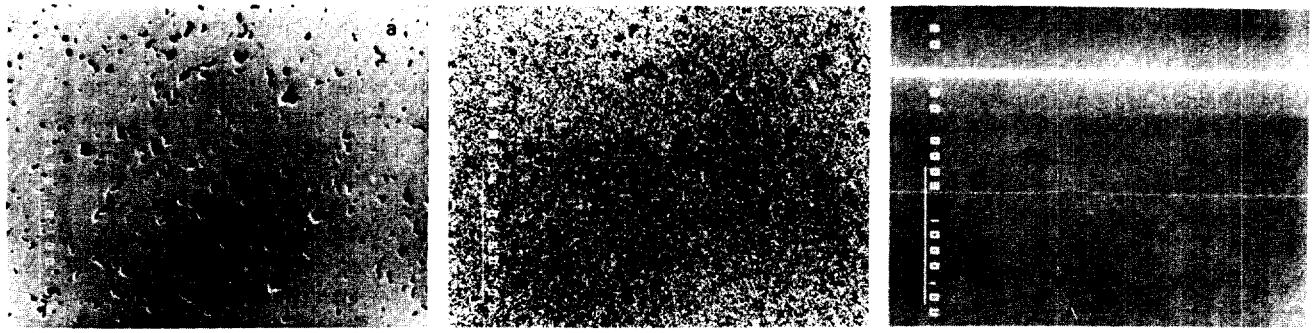

Figure 3. Homogeneous backscattered electron intensity(a), yttrium X-ray image showing homogeneous Y-distribution(b) and yttrium X-ray profile showing no significant variation of yttrium content(c) for Y123 sample.

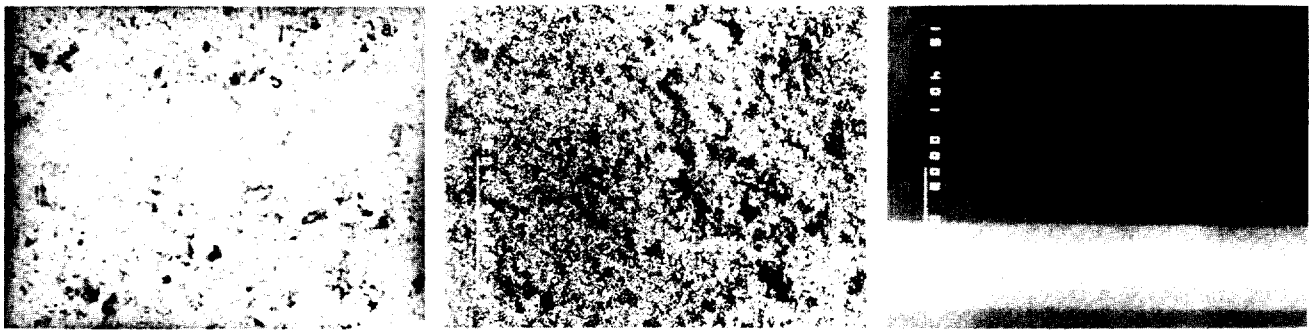

Figure 4. Homogeneous backscattered electron intensity(a), yttrium X-ray image showing homogeneous Y-distribution(b) and yttrium X-ray profile showing no significant variation of yttrium content(c) for fluorinated Y123 sample.

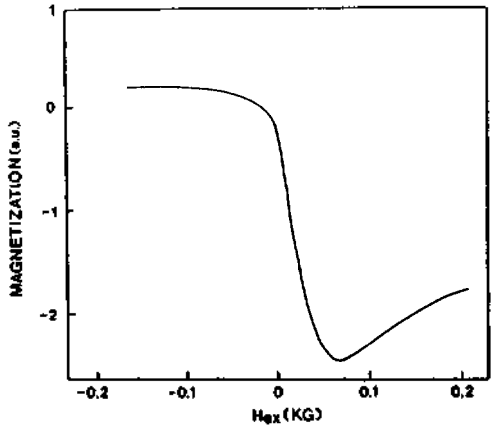

Figure 5. Magnetization curve for $YBa_2Cu_3O_{6.89}$ measured at 80 K under a low magnetic field.

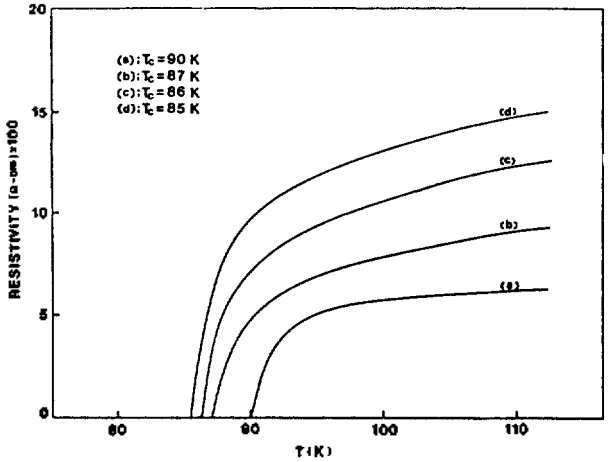

Figure 6. Temperature dependence of the resistivity for the normal and fluorinated $YBa_2Cu_3O_xF_y$ as a function of fluorine content; (a) y = 0, (b) y = 0.25, (c) y = 0.30 and (d) y = 0.35.

Y123 samples. As can be seen in Figures 3 and 4, very small dips appear in the center of the profile for the normal Y123 and in the profile for the fluorinated Y123 sample. These dips have been found to be due to the rough surfaces of the specimens. Magnified portions of the Y-distributions for the normal and fluorinated Y123 samples gave identical results and no compositional variation was detected by quantitative analysis, indicating that no microcrystal impurities exist in the $YBa_2Cu_3O_xF_y$.

Figure 5 shows the magnetization curve for $YBa_2Cu_3O_{6.89}$ measured at 80 K under a low magnetic field. An extremely large diamagnetism has been observed at temperatures as high as 80 K in superconducting $YBa_2Cu_3O_{6.89}$. The magnetization curve at 80 K was measured with a constant sweeping rate of the applied field of 250 G/min. From Figure 5, the lower critical field (H_{c1}) can be roughly estimated from the magnetization using the concept of the critical state, and Hc_1 is obtained by extrapolating the magnetization curve of an ideal type-II superconductor under a low magnetic field. From the linear part of the initial magnetization curve in the low-field region, the magnitude of the lower critical field at 80 K is estimated to be about 67 Oe for this superconducting phase. From this magnetization data, it is suggested that the magnetism can be attributed to *d*-electrons of the copper, since yttrium and barium atoms are non-magnetic. Magnetic levitations of the fluorinated Y123 samples were carried out at 77 K in air. All the resistivity curves of the fluorinated Y123 samples are similar to that of metals in the normal state at temperatures above 85 K and the resistivity decreases linearly as temperature decreases from room temperature, followed by a sharp transition to zero resistivity.

Figure 6 shows the temperature dependency of the resistivity for the normal and fluorinated Y123 samples. As can be seen in Figure 6, the onset T_c decreases as the amount of fluorine increases. This is in contrast with the result that $YBa_2Cu_3O_{7-\phi}$ with a large amount of fluorine has shown a very high superconducting temperature (150 K)[11], though it is well known that this observation has not been reproducible and higher concentrations of fluorine lead to multiphase materials which are insulating. So, it is suggested that the decrease in onset T_c with increasing fluorine concentration implies that the higher electronegativity of the fluorine substituted for the oxygen in the pyramidal Cu-O unit, compared to oxygen, increases the electronic localization of the superconducting electrons.

Acknowledgement. This paper was supported by the NON DIRECTED RESEARCH FUND, Korea Research Foundation, 1988 and partly by the Ministry of Science and Technology. The electron microprobe analyses by Professor H. S. Moon, Department of Geology, are gratefully acknowledged. The authors are grateful to Professor R. G. Sauer for helpful discussion.

References

1. R. M. Macfarlane, H. Rosen and H. Seki, *Solid State Com-*

mun., **63**, 831 (1987).
2. Y. Dai, J. S. Swinnea, H. Steinfink, J. B. Goodenough and A. Campion, *J. Am. Chem. Soc.*, **109**, 5291 (1987).
3. Z. Iqbal, S. W. Steinhauser, A. Bose, N. Cipollini and H. Eckhardt, *Phys. Rev.*, **B36**, 2283 (1987).
4. S. K. Cho, D. Kim, J. S. Choi and K. H. Kim, *J. Phys. Chem. Solids*, **51**, 113 (1990).
5. H. Rosen, E. M. Engler, T. C. Strand, V. Y. Lee and D. Bethune, *Phys. Rev.*, **B36**, 726 (1987).
6. R. J. Hemley and H. K. Mao, *Phys. Rev. Lett.*, **58**, 2340 (1987).
7. A. K. Tyagi, S. J. Patwe, U. R. K. Rao and R. M. Iyer, *Solid State Commun.*, **65**, 1149 (1988).
8. S. R. Ovshinsky, R. T. Young, D. D. Allred, G. DeMaggio and G. A. Van der Leeden, *Phys. Rev. Lett.*, **58**, 2579 (1987).
9. R. N. Bhargava, S. P. Herko and W. N. Osborne, *Phys. Rev. Lett.*, **59**, 1468 (1987).
10. D. C. Harris, M. E. Hills and T. A. Hewston, *J. Chem. Ed.*, **64**, 847 (1987).
11. K. Takeshi, *Japan–U. S. Symposium on High Temperature Superconductivity*, pp. 13–8 (1987).

Theoretical Studies on the A2 Hydrolysis of Methyl Acetimidate[1]

Ikchoon Lee*, Chang Kon Kim, and Bon-Su Lee

Department of Chemistry, Inha University, Inchon 402-751. *Received November 13, 1989*

Various mechanistic aspects of the A2 hydrolysis of methyl acetimidate were explored using the MNDO method. As in the corresponding reactions of acetamide and methyl carbamate, a proton transfer pre-equilibrium exists between the N-protonated and the O-protonated tautomers, and the subsequent hydrolysis proceeds from the more stable N-protonated form. Of the two reaction pathways, the $A_{AL}2$ path is favored in the gas phase and in concentrated acid solutions, whereas the $A_{AC}2$ path is favored in less acidic solutions with a stable cationic tetrahedral intermediate formed in the rate determining step. Negative charge development on the alkoxy oxygen in the transition state suggested a rate increase with the increase in the electron withdrawing power of the alkoxy group. Calculations on the reaction processes with AM1 indicated that MNDO is more reliable in this type of work, although AM1 is better than MNDO in reproducing hydrogen bonds.

Introduction

The interest in the solution phase studies on the acid hydrolysis of imidate ester[2-7] has long been centered around the reality of a tetrahedral addition intermediate[2-14] ((I) in Scheme 1) believed to participate in the $A_{AC}2$ hydrolysis of carbonyl compounds[15] and its implications for the mechanism of ester aminolysis.[16-18] Unlike in the $A_{AC}2$ hydrolysis of carbonyl compounds such as amides and carbamates, it is now well established that in the $A_{AC}2$ hydrolysis of imidate esters the tetrahedral addition complex, (I), constitutes a key intermediate in the course of reaction. Moreover, it has been experimentally shown that two competing pathways are possible for the imidate hydrolysis in acid solution, giving either ester and amine products by an attack of water on the acyl carbon ($A_{AC}2$ process) or amide and alcohol by an S_N2 displacement of water at the alkoxy R ($A_{AL}2$ process) of the N-protonated form of imidate esters (Scheme 1). The acid hydrolysis of 2,6-dimethylbenzimidate, which has a sterically hindered acyl carbon, has been shown to proceed predominantly (99%) by the $A_{AL}2$ pathway,[19] while that of methylbenzimidate involves partial $A_{AL}2$ process in relatively concentrated acid solution (18% $A_{AL}2$ hydrolysis in 65% H_2SO_4 solution).[20] Results of solution phase studies have also shown an enhancement of the hydrolysis rate with an increase in the electron withdrawing power of the alkoxy group of imidate esters.[21]

However we are not available the *ab initio* MO results and the gas-phase experimental data of the imidate hydrolysis or related works.

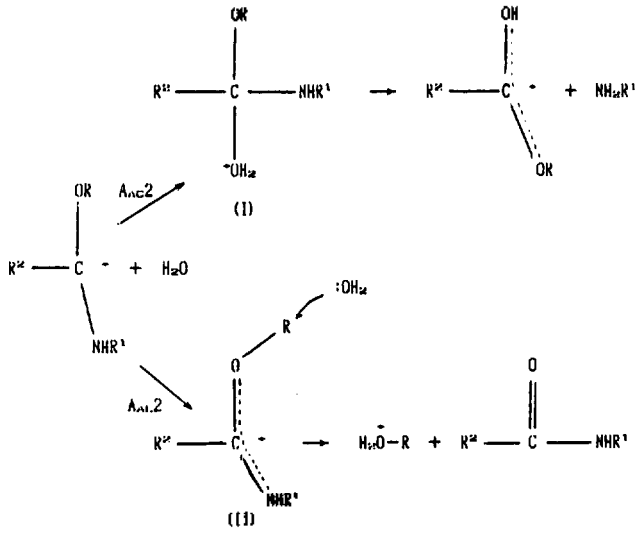

Scheme 1

In this work, we investigated the acid hydrolysis of methyl acetimidate MO theoretically using the MNDO and AM1 method[22,23] in order to explore various mechanistic possibilities and to elucidate substituent and solvent effects on the rate and mechanism of the imidate acid hydrolysis.

Calculations

Standard MNDO program[24] was used throughout in this work. Geometrical parameters of all stationary point struc-